Solar Energy
And Sustainable Development
Refereed, biannual scientific journal issued by:
The Libyan Center for Solar Energy Research and Studies

Theoretical Insights into a High-Performance Optical Absorption in GaSeS/InSeS 2D van der Waals Heterostructure for Photovoltaic Applications

Hanan Ziani[1*], Kamal Assiouan[2], Fatima Zohra Ben Abdelouahab[3], El Hassan El Harouny[4], Mustapha El Hadri[5], Farid Ben Abdelouahab[6].

[1,2,3,4,5,6]Artificial Intelligence and Computational Physics Laboratory, Faculty of Sciences, Abdelmalek Essaadi university, Tetouan, Morocco.

E-*mail:* [1] hanane.ziani@etu.uae.ac.ma ,[2] kamal.assiouan@etu.uae.ac.ma , [3] fatimazohra.benabdelouahab@etu.uae.ac.ma , [4] elharounye@gmail.com , [5] elhadri.mustafa@gmail.com , [6] fbenabdelouahab@uae.ac.ma.

SPECIAL ISSUE ON:

The 1St International Conference on Sciences and Techniques for Renewable Energy and the Environment.
(STR2E 2025)
May 6-8, 2025 at FST-Al Hoceima-Morocco.

KEYWORDS

Density Functional Theory (DFT), Electronic structure, optical analysis, GaSeS/InSeS heterostructure, Photovoltaic devices.

ABSTRACT

Advances in heterostructure design are transforming electronic and optoelectronic technologies, with particular focus on Janus monolayer-based heterojunctions. These heterojunctions, arising from the broken symmetry of 2D materials, offer new possibilities for ultra-thin, high-performance vertical p-n heterojunction solar cells. In this study, we examine the electronic structure and optical properties of a 2D GaSeS/InSeS heterostructure, formed through van der Waals interactions, based on first-principles calculations using density functional theory (DFT). The heterostructure consists of Janus group III chalcogenide GaSeS and InSeS monolayers (MLs).

The electronic properties show that both the AA and AB stacking configurations exhibit indirect semiconductor band gaps, with values of 1.3207 eV and 1.3452 eV using the PBE (Perdew-Burke-Ernzerhof) functional, and 2.0997 eV and 2.1242 eV using the Heyd-Scuseria-Ernzerhof (HSE06) hybrid functional, respectively.

Both configurations also display the characteristic features of type-II heterojunctions, which promote efficient separation of photogenerated electrons and holes. Charge density analysis reveals a transfer of charge from GaSeS to InSeS. Furthermore, optical analysis shows that both stacking configurations (AA and AB) exhibit similar absorbance spectra, primarily in the UV range, with peak absorption around 11.6×10^5 cm^{-1}. Within the visible spectrum, the maximum absorption rate for both configurations is 2.8×10^5 cm^{-1}. The 2D GaSeS/InSeS heterostructure holds great

*Corresponding author.

DOI: https://doi.org/10.51646/jsesd.v14iSTR2E.986

potential as a high-performance material for future photovoltaic devices, with promising applications in both photovoltaic cells and optoelectronic systems.

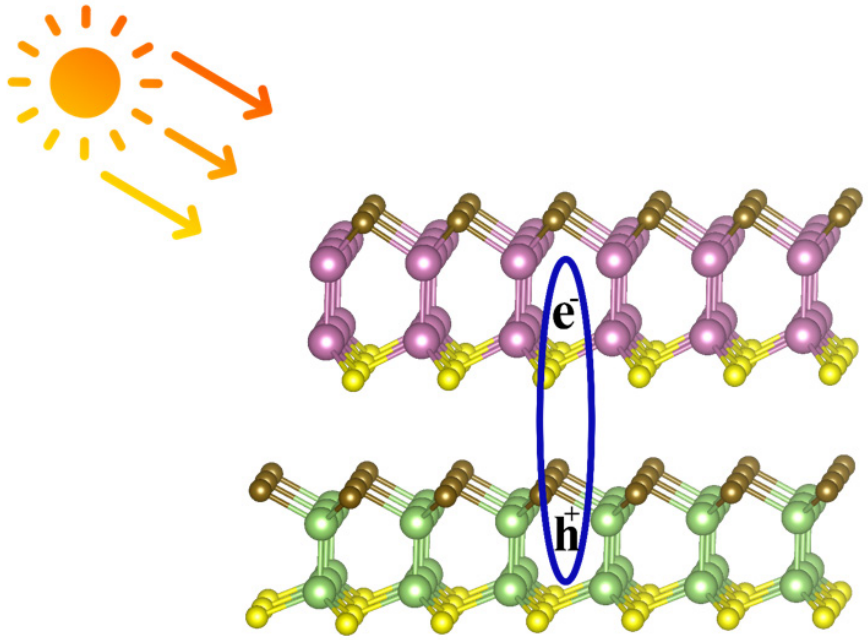

Graphical abstract.

رؤى نظرية حول الامتصاص البصري عالي الأداء في البنية المتغايرة GaSeS/InSeS 2D van der Waals للتطبيقات الكهروضوئية

حنان الزياني، كمال أسوان ، فاطمة الزهراء بن عبد الوهاب ، حسن الهاروني ، مصطفى الحضري ، فريد بن عبد الوهاب.

ملخص: تُحدث التطورات في تصميم الهياكل غير المتجانسة تحولاتٍ جذرية في التقنيات الإلكترونية والبصرية، مع التركيز بشكل خاص على الوصلات غير المتجانسة القائمة على طبقة جانوس أحادية. تُتيح هذه الوصلات غير المتجانسة، الناتجة عن اختلال تماثل المواد ثنائية الأبعاد، إمكانياتٍ جديدةً لخلايا شمسية عمودية فائقة الرقة وعالية الأداء ذات وصلات غير متجانسة p-n.

في هذه الدراسة، ندرس البنية الإلكترونية والخصائص البصرية لهيكل غير متجانس ثنائي الأبعاد من InSeS/GaSeS، مُشكّل من خلال تفاعلات فان دير فالس، استنادًا إلى حسابات المبادئ الأولية باستخدام نظرية الكثافة الوظيفية (DFT). يتكون الهيكل غير المتجانس من كالكوجينيد المجموعة الثالثة من جانوس بين طبقات أحادية (MLs) من GaSeS و InSeS. تُظهر الخصائص الإلكترونية أن تكويني التراص AA و AB يُظهران فجوات نطاق أشباه الموصلات غير المباشرة، بقيم 1.3207 إلكترون فولت و1.3452 إلكترون فولت باستخدام دالة (PBE) بيرديو-بيرك-إرنزرهو، و2.0997 إلكترون فولت و2.1242 إلكترون فولت باستخدام دالة هايد-سكوسيريا-إرنزرهوف الهجينة (HSE06)، على التوالي. كما يُظهر كلا التكوينين السمات المميزة للوصلات غير المتجانسة من النوع الثاني، والتي تُعزز الفصل الفعال للإلكترونات والفجوات المولدة ضوئيًا. يكشف تحليل كثافة الشحنة عن انتقال الشحنة من GaSeS إلى InSeS.

علاوة على ذلك، يُظهر التحليل البصري أن كلا تكويني التراص AA و AB يُظهران أطياف امتصاص متشابهة، في نطاق الأشعة فوق البنفسجية بشكل أساسي، مع ذروة امتصاص حوالي 11.6×10^5 سم$^{-1}$. في الطيف المرئي، يبلغ أقصى معدل امتصاص لكلا التكوينين $2.8 \times 11.6 \times 10^5$ سم$^{-1}$. تتمتع البنية غير المتجانسة ثنائية الأبعاد InSeS/GaSeS بإمكانيات هائلة كمواد عالية الأداء لأجهزة الطاقة الكهروضوئية المستقبلية، مع تطبيقات واعدة في كل من الخلايا الكهروضوئية والأنظمة البصرية الإلكترونية.

الكلمات المفتاحية – نظرية الكثافة الوظيفية DFT، البنية الإلكترونية، التحليل البصري، البنية غير المتجانسة لـ GaSeS/InSeS، الأجهزة الكهروضوئية.

1. INTRODUCTION

Graphite exfoliation into 2D graphene sheets has provided the scientific community with a remarkable material due to its mechanical and electronic characteristics [1].

For that, graphene is one of the most extensively researched materials among a much larger family of layered materials that can be isolated into 2D sheets, such as hexagonal boron nitride (h-BN) [2-4], transition metal dichalcogenides (TMDs) [5-8], blue or black phosphorus [9,10], and 2D Janus materials [11].

These 2D materials have drawn significant attention from the scientific community as progress in their fabrication through exfoliation or direct growth has advanced. Consequently, they exhibit multiple distinctive properties, including extremely thin dimensions, adjustable energy gaps, and exceptional mechanical attributes [12].

Nevertheless, specific imperfections in these substances, like the null energy gaps of graphene [13] and the readily corroded black phosphorus [14], Poor charge transport in TMDs leads to extended reaction durations and diminished signal-to-noise proportions [15], have restricted their possible utilizations.

To address these challenges, diverse approaches have been devised, including molecular adsorption [16-18], electrostatic field application [19-22], strain manipulation [23,24], doping [25], the formation of van der Waals heterostructures (vdWHs) [26,27], to modify the physical characteristics of 2D materials. One of the most effective strategies to address these challenges is the construction of heterostructures, which not only preserves the outstanding properties of the individual materials but also introduces new physical phenomena. This approach has proven to be both highly efficient and experimentally viable [28,29].

2D Stacked material are featured by weak van der Waals (vdW) forces between sheets, which ease the parameter alignment constraints for epitaxy and allow the production of complex vdW heterostructures [30]. This also enables new growth platforms that are difficult to achieve with conventional 3D materials. paving the way for numerous new applications, particularly such as solar photovoltaics [31,32], photodetection [33], catalytic processes [34], thermoelectric systems [35], and tunneling-based field-effect transistors [36].

For instance, many 2D van der Waals heterostructures (vdWHs) have attracted considerable interest due to their outstanding properties. For example, the $MoSe_2/PtS_2$ 2D vdW heterostructure has demonstrated exceptional optical and electronic characteristics [37,38]. Similarly, heterostructures such as graphene/phosphorene [39,40], graphene/MoS_2 [41,42], and phosphorene/MoS_2 [42,43] have gained significant attention in both theoretical and experimental studies. These structures not only retain the intrinsic properties of their individual monolayers but also offer novel or enhanced optoelectronic functionalities while remaining experimentally viable.

Recently, Janus materials have attracted considerable interest because of their unique geometry and properties [44-46]. Theoretical analyses show that monolayer MoSSe is a semiconductor with a direct band gap of 1.72 eV [45], ideal for optical absorption, and it has been successfully created by sulfurizing a $MoSe_2$ monolayer [44]. This demonstrates its potential in optoelectronic applications, especially in charge transfer and separation [46].

In a similar manner, Janus group-III monochalcogenide monolayers, represented as M_2XY (M = Ga, In; X/Y = S, Se, Te), display excellent energetic and dynamic stability [47] and also demonstrate promising optoelectronic characteristics [47,48].

For instance, In_2SeTe, In_2STe, Ga_2SeTe, and Ga_2STe have shown potential for photocatalysis [49] and can be modified by biaxial strain to engineer the optoelectronic properties of the Ga_2SSe Janus monolayer [50]. However, their relatively low photocatalytic efficiency [47] significantly limits their practical applications. Hence, improving the optoelectronic performance of group-

III monochalcogenide Janus monolayers is crucial. For example, vdW heterostructures such as In_2SeTe/Ga_2STe [51] exhibit strong optical absorption and a direct bandgap, positioning them as promising candidates for advanced solar cells. Herein, we investigate the architecture and optoelectronic characteristics of a vertical heterostructure with two stacking models, AA and AB, between GaSeS and InSeS monolayers, using first-principles simulations. The computed results indicate that both models exhibit type II band alignment. Our analysis of the optoelectronic properties of the lateral heterostructure composed of group-III monochalcogenide Janus monolayers offers valuable insights for the development and implementation of optoelectronic devices.

2. METHODOLOGY

In this present work, electronic and optical absorption calculations for GaSeS/InSeS van der Waals heterostructures were conducted through the use of density functional theory (DFT) within the Quantum ESPRESSO package [52].

The PAW (projector-augmented wave) approach [53] was utilized to include the influence of exchange-correlation contributions, alongside the PBE (Perdew-Burke-Ernzerhof) functional based on the generalized gradient approximation (GGA) [54].

The electronic and optical characteristics are carried out with a kinetic energy cutoff of 70 Ry. The Heyd-Scuseria-Ernzerhof (HSE06) hybrid functional [55] was applied to refine the electronic band structure calculations. A Gaussian broadening of 0.05 eV are utilized, and the convergence criterion for the self-consistent process are set at a total energy difference of 5×10^{-6} eV between consecutive iterations. A $12 \times 12 \times 1$ k-point grid is generated using the Monkhorst-Pack scheme to sample the first Brillouin zone [56].

To avoid interference between neighboring layers, a vacuum space of 26 Å are introduced over the axis of z. A $12\times 12 \times 1$ k-point grid is utilized to achieve static self-consistency and perform Projected density of states (PDOS) calculations along with optical property analysis.

The optical properties, including the real Re ($\varepsilon(\omega)$) and imaginary Im ($\varepsilon(\omega)$) components of the dielectric function, absorption coefficient $\alpha(\omega)$, and reflectivity, were calculated using the random phase approximation (RPA) implemented in the YAMBO code [57].

The absorption coefficient is given by Equation 1 [58]:

$$\alpha(\omega) = \frac{2\omega}{c}\left(\frac{\sqrt{\varepsilon_1^2 + \varepsilon_2^2} - \varepsilon_1}{2}\right)^{\frac{1}{2}} \qquad (1)$$

where $\varepsilon_1(\omega)$ and $\varepsilon_2(\omega)$ represent the real and imaginary parts of the complex dielectric function, respectively. XCrySDen [59] software was used to visualize the charge density variation and the optimized structures.

3. RESULTS AND ANALYSIS

3.1. Properties related to structure and stability

Before assembling the GaSeS/InSeS heterostructure, we initially examine the structural properties of the individual GaSeS and InSeS monolayers, as summarized in Table 1. Earlier investigations [47,49] have indicated that both monolayers exhibit exceptional stability, as confirmed by the absence of imaginary phonon modes. The geometric structure of GaSeS and InSeS monolayers is derived from their pristine counterparts, GaSe and InSe, which have been both theoretically studied and experimentally synthesized. These materials have been confirmed as suitable candidates for device applications due to their high absorption in the UV-visible range, significant carrier mobility, and wide band gap [47,60-62].

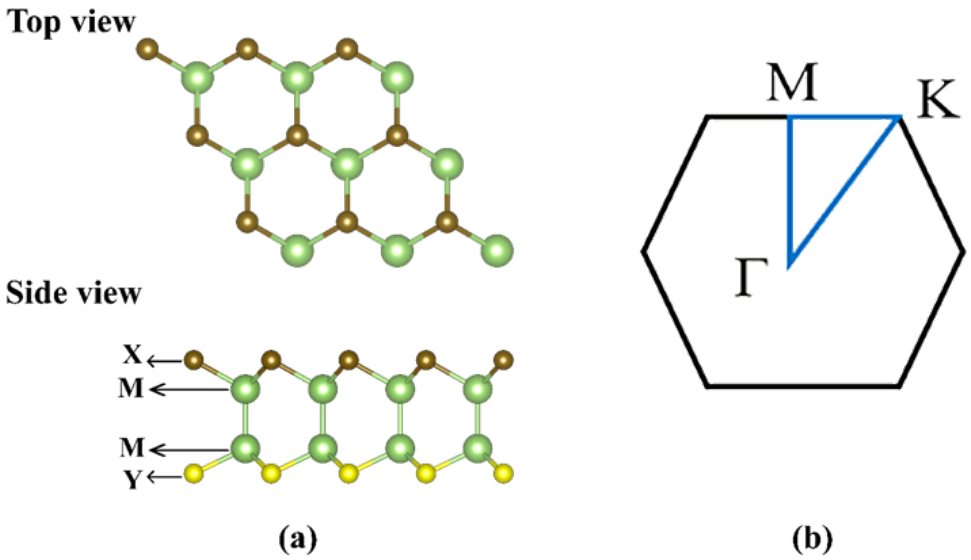

Figure 1. (a) Displays the top and side views of the 2D Janus material and (b) illustrates the Brillouin zone graph of the hexagonal structure.

Both monolayers crystallize in a hexagonal lattice with the symmetry group P3M1, and their respective Brillouin zones include high-symmetry points labeled as (Γ-M-K-Γ) (see Figure1). The optimized structural parameters, illustrated in Figure 2 (a) and (b), reveal that the equilibrium lattice constants are 3.71 Å for GaSeS and 3.89 Å for InSeS (see Table 1).

Furthermore, the band gap energies, calculated using both PBE and HSE approximations, are found to be 2.03 eV (3.07 eV) for GaSeS and 1.548 eV (2.40 eV) for InSeS, respectively, as presented in Table 1. These findings align closely with previously documented results [47,48]. Based on these results, InSeS can be considered a promising donor material for solar cell applications. The optimal band gap energy for solar cells is approximately 1.5 eV, as it falls within the primary energy range of the solar radiation. [63]

Next, we optimized the geometric structure and optoelectronic properties of the GaSeS/InSeS heterostructure, as depicted in Figure 2 (c) and (d).

Two distinct stacking configurations, AA and AB, are illustrated in these figures, showing both top and side views. The heterostructure was constructed by combining the unit cells of GaSeS and InSeS monolayers (MLs), resulting in a supercell comprising eight atoms.

To assess the lattice mismatch within the heterostructure, we employed Equation (2) [64]:

$$\delta = \left(a_{InSeS} - a_{GaSeS}\right) / a_{InSeS} \qquad (2)$$

where a_{InSeS} and a_{GaSeS} represent the refined lattice parameters of the InSeS and GaSeS monolayers, respectively.

Our calculations revealed a lattice mismatch of approximately 4.6%. Experimentally, this value remains below 5%, indicating favorable conditions for the fabrication of van der Waals (vdW) heterostructures [65].

As shown in Figure 2(c), the interlayer distance for the AA-stacked configuration is determined by the S–Se interaction, measuring 2.24 Å.

In contrast, for the AB-stacked configuration, the interlayer distance corresponds to the Se–In interaction, measuring 2.98 Å (see Figure2).

The optimized lattice constants were calculated as 3.86 Å for the AA configuration and 3.87 Å for the AB configuration. (see Table 1)

To evaluate the energetic stability of the GaSeS/InSeS heterostructure, we computed the interlayer binding energy using Equation (3) [66]:

$$E_b = E_{GaSeS/InSeS} - \left(E_{GaSeS} + E_{InSeS}\right) \quad (3)$$

where $E_{GaSeS/InSeS}$, E_{GaSeS}, and E_{InSeS} correspond to the total energies of the GaSeS/InSeS heterostructure, the GaSeS monolayer, and the InSeS monolayer, respectively.

A binding energy of –0.31 eV was obtained for both AA and AB configurations as shown in Table 1, confirming the thermodynamic stability of the heterostructure.

These binding energy values are comparable to previous results for WSSe-WS_2 (-0.350 eV), WSSe-WSe_2 (-0.492 eV) [67], BP/MoS_2 (-1.23 eV) [68], and Janus group-III chalcogenides (-31.68 eV) [69]. This highlights their role in enhancing the stability of vertical heterostructures, ensuring epitaxial quality and improved physical properties.

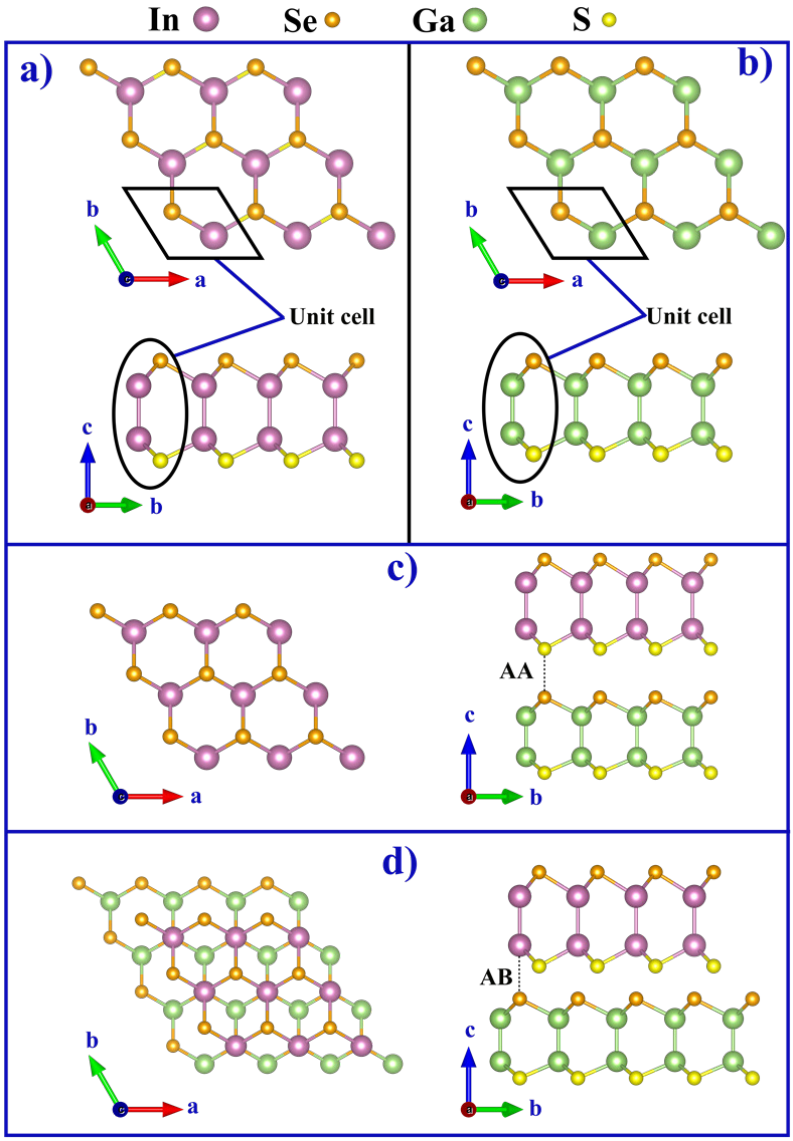

Figure 2. Schematic representation of the optimized structure, showing the top and side views of (a) InSeS and (b) GaSeS monolayers, as well as the GaSeS/InSeS heterostructures in (c) AA-stacking and (d) AB-stacking configurations.

Table 1. Computed lattice constants (in Å), binding energy (eV), electronic bandgap Eg (PBE and HSE (in eV) and interlayer distance Dinter for heterostructure (in Å).

system	a	E_b	E_g^{PBE}	E_g^{HSE}	D_{inter}	Ref.
GaSeS	3.71 3.73 3.72	-	2.03	3.07 2.91 2.97	-	This work [47] [49]
InSeS	3.89 4.01 4.00	-	1.54	2.40 2.28 2.34	-	This work [47] [49]
GaSeS/InSeS AA-stacking	3.86	- 0.31	1.32	2.09	2.24	This work
GaSeS/InSeS AB-stacking	3.87	- 0.31	1.36	2.12	2.98	This work
Al_2OS/Ga_2SSe	3.7	-22.8 meV/Å2	-	2.34	-	[73]
$In_2SeS/g\text{-}C_3N_4$	-	-2.21	-	2.03	3	[76]

3.2. Electronic properties

The electronic band structure plays a crucial role in defining the characteristics of materials for photovoltaic solar cell applications. Figures 3 and 4 illustrate the energy bands alongside the projected density of states (PDOS) for the GaSeS and InSeS monolayers, as well as for the GaSeS/InSeS van der Waals heterostructure (vdWH) for two AA and AB stacking.

Figure 3 (a, c) presents the band structures of the GaSeS and InSeS monolayers obtained using the HSE approximation. Table 1 summarizes the calculated energy band gaps for both PBE and HSE approximations, showing that GaSeS has an indirect band gap of 2.03 eV with the PBE method and 3.07 eV with the HSE06 approach. Similarly, the InSeS monolayer exhibits an indirect band gap of 1.54 eV (PBE) and 2.4 eV (HSE06), both positioned between the conduction and valence bands. In both cases, the indirect band gap is located between the Γ point in the conduction band and between the Γ and M points in the valence band.

The obtained band gap value for the GaSeS monolayer aligns closely with previous literature, which reports a value of 2.04 eV [49,69]. However, the calculated band gap for the InSeS monolayer is higher than that reported in earlier studies [49] However, it remains comparable to the experimental values for the original InSe and GaSe monolayers [70,71].

The electronic band structure of the GaSeS/InSeS van der Waals heterostructure were analyzed for two stacking configurations (AA and AB) using the HSE hybrid functional and PBE functional, as depicted in Figure 4 (a, c). Table 1 presents the calculated energy bandgap values obtained using both PBE and HSE approximations.

The results indicate that both stacking configurations exhibit an indirect bandgap, with the conduction band minimum (CBM) located at the Γ point and the valence band maximum (VBM) along the Γ-M path, without any significant alteration of energy levels. A detailed examination of Figure 4 (a, c) reveals that the band structures of the AA and AB configurations exhibit negligible differences, with energy bandgaps of 2.09 eV and 2.12 eV, respectively with HSE approch as similar findings regarding favorable stacking positions have been reported in previous studies on GaS/GaSe [72] and $WSSe/WSe_2$ [67] heterostructures. The obtained bandgap values for GaSeS/InSeS are comparable to those reported in other works, being lower than those of Al_2OS/Ga_2SSe (2.34 eV) [73] and GaN/SiS (2.45 eV) [74] but higher than those of BP/Ga_2SSe (0.85 eV) [75], In_2SeTe/Ga_2STe (1.91 eV) [51] and $In_2SeS/g\text{-}C_3N_4$ (2.03 eV) [76].

The bandgaps calculated using the PBE approach are 1.32 eV and 1.36 eV for the AA and AB configurations, respectively, as shown in Table 1. When compared to the optimal bandgap range for a single-junction solar cell according to Shockley-Queisser theory (1.1–1.6 eV) [77], the reduced bandgap suggests improved charge carrier separation and transfer, enhancing the

material's potential for photovoltaic applications.

Furthermore, the GaSeS/InSeS heterostructure exhibits a type-II band alignment, with a valence band offset (VBO) of 0.79 eV and a conduction band offset (CBO) of 0.29 eV between the GaSeS and InSeS layers. The relatively low CBO indicates a high open-circuit voltage, which is advantageous for photovoltaic applications, as previously reported for GeAs/GaSe [78]. This band alignment is further confirmed by the projected density of states (PDOS) analysis, reinforcing the potential of GaSeS/InSeS as a promising candidate for solar cell applications.

The projected density of states (PDOS) provides insight into the contributions of atomic orbitals and their relation to the Fermi level. Figures 3 and 4 (b and d) illustrate the PDOS for GaSeS, InSeS monolayers (MLs), and GaSeS/InSeS van der Waals heterostructures (vdWHs) in AA and AB stacking configurations, respectively. In the figures, negative values represent the valence bands, while positive values indicate the conduction bands, with zero corresponding to the Fermi level [79]. The PDOS, ranging from −5 eV to 5 eV, reveals the movement of electrons from the valence to the conduction bands, as well as on the hybridization of atomic orbitals in the materials. The computed PDOS, obtained using the PBE functional, supports the band gap values derived from previous analyses. For the GaSeS and InSeS MLs, the CBM and VBM are primarily influenced by p orbitals. Specifically, the contributions to the CBM mainly originate from Ga-p and In-p orbitals, while the VBM is primarily driven by S-p and Se-p orbitals (see Figure 3 b and d). As depicted in Figure 4 (b and d), the PDOS profiles for AA and AB stacking exhibit similar trends, with slight variations in valence state intensity. The valence band is strongly influenced by the S-p and Se-p orbitals, with values ranging from 2.78 to 2.52 states/eV, while the conduction band is governed by In-p and Ga-p orbitals at 1.88 and 1.42 states/eV, respectively.

Overall, the energy band gaps extracted from the PDOS for both stacking configurations are in good agreement with those obtained from their corresponding band structures.

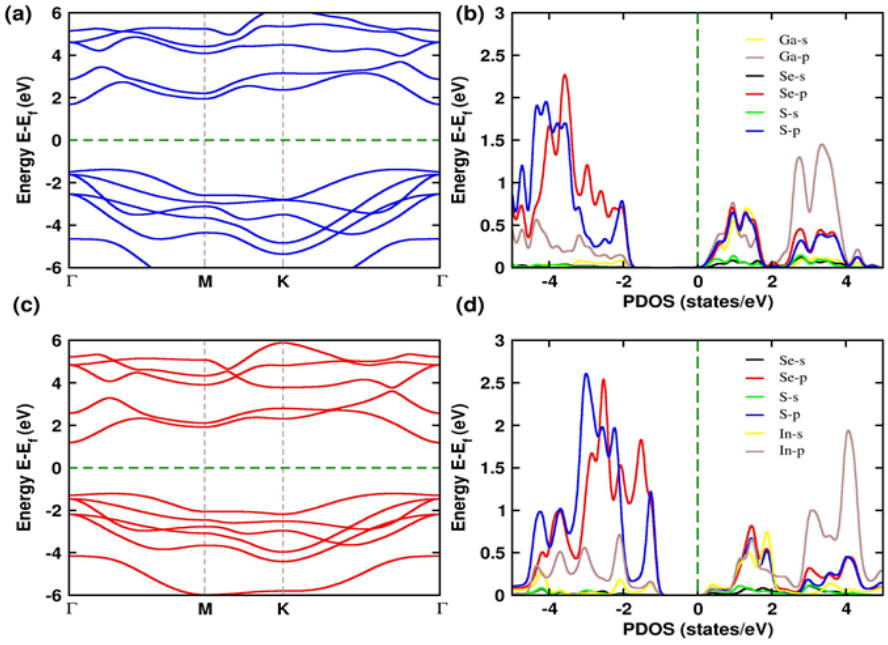

Figure 3. (a) and (c) depict the band structure calculated using the HSE functional, while (b) and (d) show the projected band structure obtained with the PBE functional for GaSeS and InSeS monolayers.

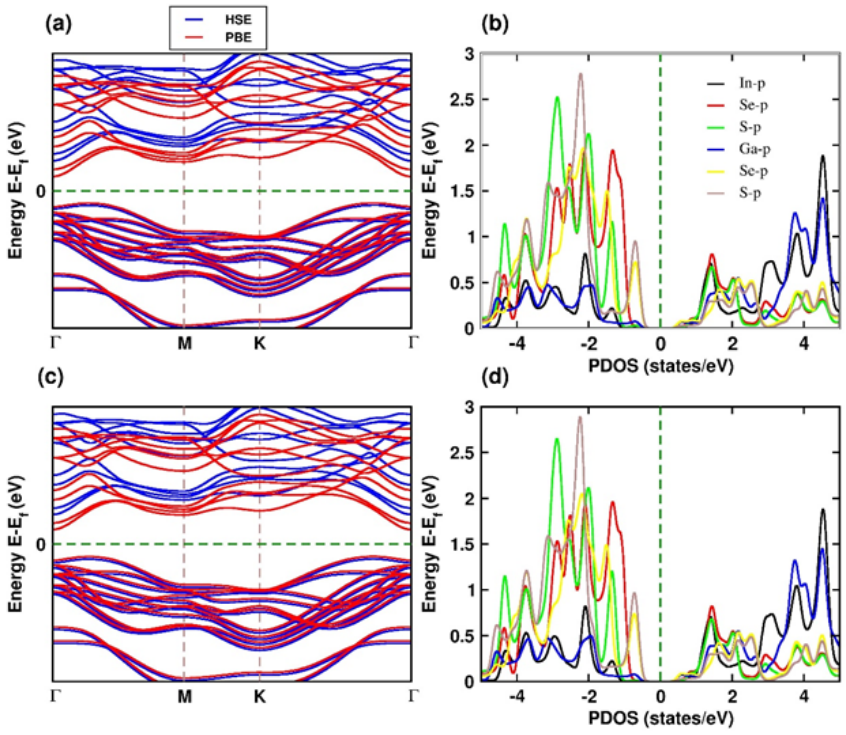

Figure 4. The band structure calculated using the (HSE &PBE) functional and the projected band structure obtained with the PBE functional for AA-stacking in (a) and (b), and AB-stacking in (c) and (d).

To analyze the movement of charge between GaSeS and InSeS monolayers in the vdWs stacked heterostructure, we evaluated the averaged z-direction planar electrostatic potential for both, AA and AB stacking (see Figure 5). Our observations indicate that, in both configurations, the InSeS-ML has a stronger energy than the GaSeS-ML, leading to a greater accumulation of electrons on the GaSeS monolayer. As given in Figure 5, the potential difference over the GaSeS/InSeS heterostructure is ΔV = 2.03 eV for the AA stacking and ΔV = 2.00 eV for the AB stacking as depicted in Figure 5 (a) and (b), respectively. This potential difference creates a built-in electric field that encourages the movement of electrons from the GaSeS monolayer to the InSeS monolayer, as well as the transfer of holes from the InSeS-ML to the GaSeS-ML.

In general, a strong built-in electric field can effectively suppress the recombination of photogenerated electron-hole pairs [79]. Compared to previous studies, the potential drop in GaSeS/InSeS is greater than that observed in Al_2OS/Ga_2SSe [73] and black-P/blue-P [80], which enhances carrier separation. Furthermore, to enhance our understanding of the electron movement at the boundary of the GaSeS/InSeS system, we analyzed the variation in charge density within the van der Waals (vdW) heterostructure. This difference is defined by the equation (4) [81]:

$$\Delta\rho = \rho\left(GaSeS\ /\ InSeS\right) - \rho\left(GaSeS\right) - \rho\left(InSeS\right) \qquad (4)$$

where ρ(GaSeS/InSeS), ρ(GaSeS), and ρ(InSeS) indicate the charge density of the heterostructure, the Janus GaSeS, and the InSeS monolayers.

Figure 6 (a) and (b) illustrate the charge density distributions for AA and AB stacking, respectively. The yellow region corresponds to an area of electron accumulation, while the cyan region corresponds to an area of electron depletion. At the interface region, charges redistribute: they accumulate near the GaSeS monolayer and deplete near the InSeS monolayer.

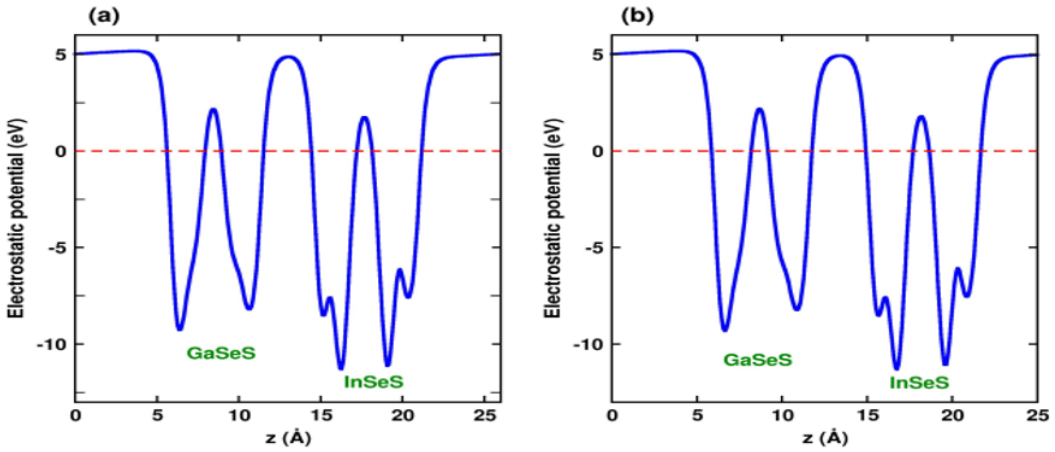

Figure 5. Electrostatic potential energy for a) AA-stacking and (b) AB-stacking of GaSeS/InSeS heterostructure.

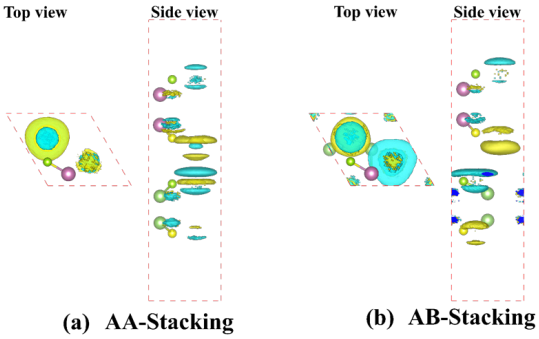

Figure 6. Visualization of the differential charge density with top and side views for (a) AA-stacking and (b) AB-stacking of the GaSeS/InSeS heterostructure.

3.3. Optical properties

A photovoltaic material should efficiently absorb sunlight and convert this energy into electron-hole pairs. Therefore, calculating its optical properties is crucial for assessing its light absorption efficiency [82].

To achieve this, we perform a detailed examination of the real (ε_1) and imaginary (ε_2) components of the dielectric response function, $\varepsilon(\omega)$, for the GaSeS/InSeS heterostructure in both AA and AB stacking configurations, as described by Equation 5 [58]:

$$\varepsilon(\omega) = \varepsilon_1(\omega) + i\varepsilon_2(\omega) \qquad (5)$$

According to Figure 7(a), the imaginary part of the dielectric response function (ε_2) reaches its highest peak at 4.14 eV, with a maximum value of 10.57 for the two-stack configuration of the GaSeS/InSeS heterostructure. Additionally, InSeS exhibits a secondary peak at 4.42 eV with a magnitude of 6.21, while GaSeS shows a lower-intensity peak at 4.42 eV with a value of 1.64.

As depicted in the inset of Figure 7(b), variations in ε_1, the real component of the dielectric response function, are analyzed for GaSeS and InSeS monolayers as well as the GaSeS/InSeS heterostructure. For both AA and AB stacking configurations of the heterostructure, the static dielectric constant $\varepsilon_1(0)$ is determined to be 4.5, indicating an enhancement compared to the individual monolayers. Moreover, distinct peaks appear in the $\varepsilon_1(\omega)$ spectrum across the visible and ultraviolet regions of the electromagnetic spectrum, corresponding to various interband transitions from the valence band maximum (VBM) to the conduction band minimum (CBM).

In addition, Figure 8 (a) illustrates the optical absorption of GaSeS and InSeS monolayers, as well as the GaSeS/InSeS heterostructure. The figure reveals that the first absorption edge, observed around 2 eV, closely matches the predicted band gaps of 2.09 eV for the AA stacking and 2.12

eV for the AB stacking. Notably, there is a strong agreement between the optical absorption coefficient and the imaginary component of the dielectric response function within the considered range. The incorporation of GaSeS and InSeS into the heterostructure significantly alters the absorption peaks, especially in the regions around 4 and 7 eV. These results clearly show that GaSeS/InSeS van der Waals heterostructures are more efficient at absorbing UV light compared to the individual monolayers.

While the maximum absorption peak value in the visible spectrum reaches 2.8×10^5 cm^{-1}, the absorption is primarily influenced by the presence of InSeS rather than GaSeS in the ultraviolet region, where the absorption peak reaches a maximum value of 11.6×10^5 cm^{-1}. These findings are consistent with those reported in the literature [48, 51, 62, 78]. The optical absorption of the vdW heterostructure remains relatively stable across different layer configurations, with only minor fluctuations [83].

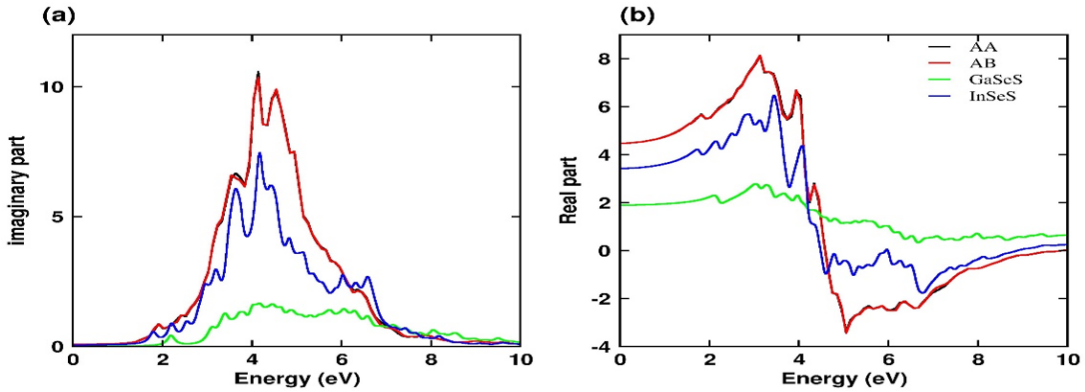

Figure 7. Imaginary ε_2 (ω) and the real ε_1(ω) components of the dielectric response function for AA-stacking and AB-stacking and Mls.

Moreover, the reflectivity coefficient R(λ) for the GaSeS/InSeS heterostructure is twice that of the individual monolayers (see Figure 8(b)), indicating that the GaSeS/InSeS vdW heterostructures hold significant potential for efficient solar cells and ultra-thin optoelectronic systems.

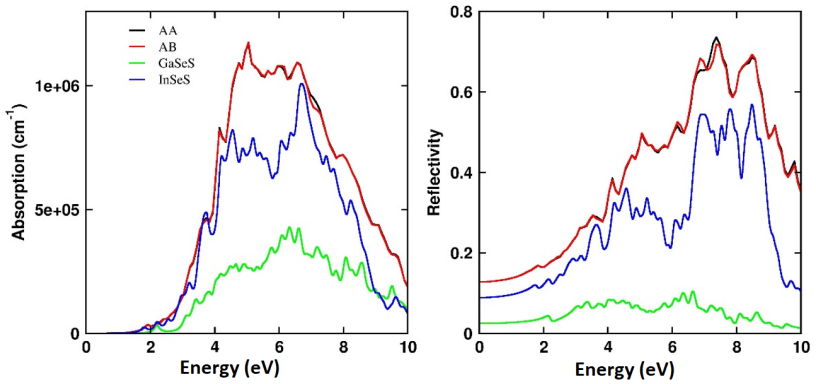

(a) (b)

Figure 8. The optical absorption and reflectivity factors for both AA and AB stacking configurations, along with the monolayer structures (MLs).

4. CONCLUSION

This study provides a comprehensive evaluation of the structural, optical, and electronic properties of the GaSeS/InSeS heterostructure, examining two stacking configurations through first-principles calculations. The results show that both stacking configurations are indirect

semiconductor band gaps, with values of 2.09 eV for AA and 2.12 eV for AB, using the HSE approximation. The heterostructure exhibits a Type-II band alignment, suggesting significant spatial separation of photogenerated carriers, which indicates its potential for use in photovoltaic device fabrication. Furthermore, substantial built-in electric fields were observed at the GaSeS/InSeS interfaces, which are expected to enhance the lifetime of photo-generated carriers. Notably, the GaSeS/InSeS heterostructure demonstrates exceptionally strong optical absorption in the visible and ultraviolet spectra, reaching up to 10^5 cm^{-1}. These results highlight the GaSeS/InSeS heterostructure as a promising candidate for solar cell applications. Our findings also offer valuable insights for guiding future experimental investigations.

Authors contribution: Ziani Hanan: Writing - Review & Editing, Conceptualization, Methodology, Software, Validation, Investigation, Writing - Original Draft, Visualization. Assiouan Kamal: Writing - Review & Editing, Formal analysis, Validation. Fatima Zohra Ben Abdelouahab: Writing, Formal analysis, Validation, Review & Editing. El Harouny El Hassan: Software, Formal analysis, Validation, Visualization. El Hadri Mustapha: Supervision, Formal analysis, Investigation, Validation. Ben Abdelouahab Farid: Writing - Review & Editing, Validation, Visualization.

Funding: The authors sincerely appreciate the support of "The Moroccan Association of Sciences and Techniques for Sustainable Development (MASTSD), Beni Mellal, Morocco," and extend their gratitude to its president, Professor Charaf Laghlimi, for his valuable contributions.

Data Availability Statement: Data is available on the request.

Conflicts of Interest: No conflict of interest.

Acknowledgements: The authors express their gratitude to CNRST (National Center for Scientific and Technical Research) in Rabat, Morocco, for providing access to its computational cloud resource - HPC-MARWAN.

REFERENCES

[1] C. Dean, A. F. Young, L. Wang, I. Meric, G. H. Lee, K. Watanabe, T. Taniguchi, P. Kim, K. L. Shepard, and J. Hone, "Graphene-based heterostructures," Solid State Commun., vol. 152, no. 15, pp. 1275–1282, Aug. 2012. doi: 10.1016/j.ssc.2012.04.021.

[2] J. Mawwa, S. U. D. Shamim, S. Khanom, M. K. Hossain, and F. Ahmed, "In-plane graphene/boron nitride heterostructures and their potential application as toxic gas sensors," RSC Advances, vol. 11, no. 52, pp. 32810–32823, Dec. 2021. doi: 10.1039/D1RA06304A.

[3] L. Song, L. Ci, H. Lu, P. B. Sorokin, C. Jin, J. Ni, A. G. Kvashnin, J. Lou, B. I. Yakobson, and P. M. Ajayan, "Large-scale growth and characterization of atomic hexagonal boron nitride layers," Nano Letters, vol. 10, no. 8, pp. 3209–3215, Aug. 2010. doi: 10.1021/nl1022139.

[4] L. Ci, L. Song, C. Jin, D. Jariwala, D. Wu, Y. Li, A. Srivastava, Z. F. Wang, K. Storr, L. Balicas, F. Liu, and P. M. Ajayan, "Atomic layers of hybridized boron nitride and graphene domains," Nature Materials, vol. 9, no. 5, pp. 430–435, May 2010. doi: 10.1038/nmat2711.

[5] A. Schleife, C. Rödl, F. Fuchs, J. Furthmüller, and F. Bechstedt, "Strain influence on valence-band ordering and excitons in ZnO: An ab initio study," Applied Physics Letters, vol. 91, no. 24, Dec. 2007. doi: 10.1063/1.2825277.

[6] S. Wang, M. S. Ukhtary, and R. Saito, "Strain effect on circularly polarized electroluminescence in transition metal dichalcogenides," Physical Review Research, vol. 2, no. 3, Sep. 2020. doi: 10.1103/PhysRevResearch.2.033340.

[7] M. Z. Bellus, M. Li, S. D. Lane, F. Ceballos, Q. Cui, X. C. Zeng, and H. Zhao, "Type-I van der Waals heterostructure formed by MoS_2 and ReS_2 monolayers," Nanoscale Horizons, vol. 2, no. 1,

pp. 31–36, Jan. 2017. doi: 10.1039/C6NH00144K.

[8] N. Huo, Y. Yang, and J. Li, "Optoelectronics based on 2D TMDs and heterostructures," Journal of Semiconductors, vol. 38, no. 3, p. 031002, Mar. 2017. doi: 10.1088/1674-4926/38/3/031002.

[9] X. Li, X. Wu, Z. Zhu, G. Li, and C. Mi, "On the elasticity and piezoelectricity of black (blue) phosphorus/ZnO van der Waals heterostructures," Computational Materials Science, vol. 169, p. 109134, Sep. 2019. doi: 10.1016/j.commatsci.2019.109134.

[10] T. Sahdane, S. Mtougui, F. Goumrhar, N. Mamouni, E. Salmani, H. Ez-Zahraouy, and O. Mounkachi, "Magnetic phase transitions of phosphorene-like nano-structure: Monte Carlo study," Philosophical Magazine, vol. 101, no. 16, pp. 1836–1848, Jun. 2021. doi: 10.1080/14786435.2021.1936260.

[11] J. Seeyangnok, M. U. Hassan, U. Pinsook, and G. J. Ackland, "Superconductivity and electron self-energy in tungsten-sulfur-hydride monolayer," 2D Materials, vol. 11, no. 2, p. 025020, Mar. 2024. doi: 10.1088/2053-1583/ad2523.

[12] N. Thakur, P. Kumar, S. Kumar, A. K. Singh, H. Sharma, N. Thakur, and P. Sharma, "A review of two-dimensional inorganic materials: Types, properties, and their optoelectronic applications," Progress in Solid State Chemistry, p. 100443, Feb. 2024. doi: 10.1016/j.progsolidstchem.2024.100443.

[13] M. Li, L. Wang, N. Yu, X. Sun, T. Hou, and Y. Li, "Structural stability and band gap tunability of single-side hydrogenated graphene from first-principles calculations," Journal of Materials Chemistry C, vol. 3, no. 15, pp. 3645–3649, Apr. 2015. doi: 10.1039/C5TC00209E.

[14] J. M. Hamm and O. Hess, "Two two-dimensional materials are better than one," Science, vol. 340, no. 6138, pp. 1298–1299, Jun. 2013. doi: 10.1126/science.1239501.

[15] K. Kaasbjerg, T. Low, and A. P. Jauho, "Electron and hole transport in disordered monolayer MoS_2: Atomic vacancy induced short-range and Coulomb disorder scattering," Physical Review B, vol. 100, no. 11, p. 115409, Sep. 2019. doi: 10.1103/PhysRevB.100.115409.

[16] K. Yang, Z. Cui, E. Li, Y. Shen, L. Zhang, D. Ma, Y. Liu, L. Yang, Z. Wu, W. Zhou, and S. Zhang, "Modulation of the magnetic, electronic, and optical behaviors of WS_2 after metals adsorption: A first-principles study," Chemical Physics, vol. 571, p. 111903, 2023, doi: 10.1016/j.chemphys.2023.111903.

[17] C. H. Hung, Y. C. Jiang, S. Y. Lei, R. Gao, X. W. Tao, N. Wan, and H. Yu, "Small gas adsorption on 2D material SnSe: A first-principles study," Journal of Physics D: Applied Physics, vol. 56, no. 39, p. 395302, 2023, doi: 10.1088/1361-6463/ace195.

[18] A. S. Alsaman, H. Maher, M. Ghazy, E. S. Ali, A. A. Askalany, and B. B. Saha, "2D materials for adsorption desalination applications: A state of the art," Thermal Science and Engineering Progress, vol. 49, p. 102455, 2024, doi: 10.1016/j.tsep.2024.102455.

[19] K. Rahimi, "Electric-field-and strain-induced adjustability of vdW heterostructure of g-ZnO/2H-TiS_2 for optoelectronic applications," Materials Letters, vol. 282, p. 128680, Jan. 2021. doi: 10.1016/j.matlet.2020.128680.

[20] Y. Cheng, L. Li, L. Li, Y. Zhang, L. Wang, L. Wang, and Y. Gao, "Linear regulation of electrical characteristics of InSe/Antimonene heterojunction via external electric field and strain," Surfaces and Interfaces, vol. 23, p. 101014, Jun. 2021. doi: 10.1016/j.surfin.2021.101014.

[21] X. P. Wang, X. B. Li, N. K. Chen, J. H. Zhao, Q. D. Chen, and H. B. Sun, "Electric field analyses on monolayer semiconductors: The example of InSe," Physical Chemistry Chemical Physics, vol. 20, no. 10, pp. 6945–6950, Mar. 2018. doi: 10.1039/C7CP07270H.

[22] Z. Yang and J. Ni, "Modulation of electronic properties of hexagonal boron nitride bilayers by

an electric field: A first principles study," Journal of Applied Physics, vol. 107, no. 10, May 2010. doi: 10.1063/1.3373571.

[23] C. Shi, Q. Song, H. Wang, S. Ma, C. Wang, X. Zhang, and Q. Chen, "Molecular hinges stabilize formamidinium-based perovskite solar cells with compressive strain," Advanced Functional Materials, vol. 32, no. 28, p. 2201193, Jul. 2022. doi: 10.1002/adfm.202201193.

[24] Y. Hu, S. Zhang, S. Sun, M. Xie, B. Cai, and H. Zeng, "GeSe monolayer semiconductor with tunable direct band gap and small carrier effective mass," Applied Physics Letters, vol. 107, no. 12, Sep. 2015. doi: 10.1063/1.4931459.

[25] G. Guo, Y. Shi, Y. Zhang, Y. Deng, F. Du, Z. Xie, and Y. Mao, "First-principles study on the electronic and magnetic properties of P edge-doped armchair germanium selenide nanoribbon," Computational Materials Science, vol. 172, p. 109348, Jan. 2020. doi: 10.1016/j.commatsci.2019.109348.

[26] X. Liu and M. C. Hersam, "Interface characterization and control of 2D materials and heterostructures," Advanced Materials, vol. 30, no. 39, p. 1801586, 2018, doi: 10.1002/adma.201801586.

[27] R. Long and O. V. Prezhdo, "Quantum coherence facilitates efficient charge separation at a MoS_2/$MoSe_2$ van der Waals junction," Nano Letters, vol. 16, no. 3, pp. 1996–2003, Mar. 2016. doi: 10.1021/acs.nanolett.5b05264.

[28] M. Luo, Y. E. Xu, and Y. X. Song, "Tunable electronic properties of MoS_2/ReS_2 van der Waals heterostructure from first-principles study," Optik, vol. 144, pp. 334–339, Sep. 2017. doi: 10.1016/j.ijleo.2017.06.100.

[29] K. Zhang, C. Ding, Y. She, Z. Wu, C. Zhao, B. Pan, and Q. Fan, "$CuFe_2O_4$/MoS_2 mixed-dimensional heterostructures with improved gas sensing response," Nanoscale Research Letters, vol. 15, p. 7, Jan. 2020. doi: 10.1186/s11671-020-3268-4.

[30] Y. Gong, J. Lin, X. Wang, G. Shi, S. Lei, Z. Lin, and P. M. Ajayan, "Vertical and in-plane heterostructures from WS_2/MoS_2 monolayers," Nature Materials, vol. 13, no. 12, pp. 1135–1142, Dec. 2014, doi: 10.1038/NMAT4091.

[31] M. J. Molaei, M. Younas, and M. Rezakazemi, "Van der Waals heterostructures in ultrathin 2D solar cells: State-of-the-art review," Materials Science and Engineering: B, vol. 285, p. 115936, 2022, doi: 10.1016/j.mseb.2022.115936.

[32] P. Wang, X. Li, Z. Xu, Z. Wu, S. Zhang, W. Xu, and S. Lin, "Tunable graphene/indium phosphide heterostructure solar cells," Nano Energy, vol. 13, pp. 509–517, 2015, doi: 10.1016/j.nanoen.2015.03.023.

[33] F. Yan, C. Hu, Z. Wang, H. Lin, and K. Wang, "Perspectives on photodetectors based on selenides and their van der Waals heterojunctions," Applied Physics Letters, vol. 118, no. 19, 2021, doi: 10.1063/5.0045941.

[34] S. Wang, C. Ren, H. Tian, J. Yu, and M. Sun, "MoS_2/ZnO van der Waals heterostructure as a high-efficiency water splitting photocatalyst: A first-principles study," Physical Chemistry Chemical Physics, vol. 20, no. 19, pp. 13394–13399, 2018, doi: 10.1039/C8CP00808F.

[35] R. D'Souza and S. Mukherjee, "Thermoelectric transport in graphene/h-BN/graphene heterostructures: A computational study," Physica E: Low-dimensional Systems and Nanostructures, vol. 81, pp. 96–101, 2016, doi: 10.1016/j.physe.2016.03.006.

[36] L. Britnell, R. V. Gorbachev, R. Jalil, B. D. Belle, F. Schedin, A. Mishchenko, and L. A. Ponomarenko, "Field-effect tunneling transistor based on vertical graphene heterostructures,"

Science, vol. 335, no. 6071, pp. 947–950, 2012, doi: 10.1126/science.1218461.

[37] A. O. M. Almayyali, B. B. Kadhim, and H. R. Jappor, "Stacking impact on the optical and electronic properties of two-dimensional $MoSe_2/PtS_2$ heterostructures formed by PtS_2 and $MoSe_2$ monolayers," Chemical Physics, vol. 532, p. 110679, 2020, doi: 10.1016/j.chemphys.2020.110679.

[38] A. O. M. Almayyali, B. B. Kadhim, and H. R. Jappor, "RETRACTED: Tunable electronic and optical properties of 2D PtS_2/MoS_2 van der Waals heterostructure," Physica E: Low-dimensional Systems and Nanostructures, vol. 113, p. 113866, 2020, doi: 10.1016/j.physe.2019.113866.

[39] X. Tian, L. Liu, Y. Du, J. Gu, J. B. Xu, and B. I. Yakobson, "Variable electronic properties of lateral phosphorene–graphene heterostructures," Physical Chemistry Chemical Physics, vol. 17, no. 47, pp. 31685–31692, 2015, doi: 10.1039/C5CP05443E.

[40] Y. Cai, G. Zhang, and Y. W. Zhang, "Electronic properties of phosphorene/graphene and phosphorene/hexagonal boron nitride heterostructures," The Journal of Physical Chemistry C, vol. 119, no. 24, pp. 13929–13936, 2015, doi: 10.1021/acs.jpcc.5b02634.

[41] M. T. Hossain and M. A. Rahman, "A first principle study of the structural, electronic, and temperature-dependent thermodynamic properties of graphene/MoS_2 heterostructure," Journal of Molecular Modeling, vol. 26, no. 1, pp. 1–8, 2020, doi: 10.1007/s00894-020-4306-y.

[42] W. Hu and J. Yang, "Two-dimensional van der Waals heterojunctions for functional materials and devices," Journal of Materials Chemistry C, vol. 5, no. 47, pp. 12289–12297, 2017, doi: 10.1039/C7TC04697A.

[43] P. Vishnoi, K. Pramoda, U. Gupta, M. Chhetri, R. G. Balakrishna, and C. N. R. Rao, "Covalently linked heterostructures of phosphorene with $MoS_2/MoSe_2$ and their remarkable hydrogen evolution reaction activity," ACS Applied Materials & Interfaces, vol. 11, no. 31, pp. 27780–27787, 2019, doi: 10.1021/acsami.9b06910.

[44] A. Y. Lu, H. Zhu, J. Xiao, C. P. Chuu, Y. Han, M. H. Chiu, and L. J. Li, "Janus monolayers of transition metal dichalcogenides," Nature Nanotechnology, vol. 12, no. 8, pp. 744–749, 2017, doi: 10.1038/nnano.2017.100.

[45] M. Palsgaard, T. Gunst, T. Markussen, K. S. Thygesen, and M. Brandbyge, "Stacked Janus device concepts: abrupt pn-junctions and cross-plane channels," Nano Letters, vol. 18, no. 11, pp. 7275–7281, 2018, doi: 10.1021/acs.nanolett.8b03474.

[46] A. C. Riis-Jensen, T. Deilmann, T. Olsen, and K. S. Thygesen, "Classifying the electronic and optical properties of Janus monolayers," ACS Nano, vol. 13, no. 11, pp. 13354–13364, 2019, doi: 10.1021/acsnano.9b06698.

[47] Y. Bai, Q. Zhang, N. Xu, K. Deng, and E. Kan, "The Janus structures of group-III chalcogenide monolayers as promising photocatalysts for water splitting," Applied Surface Science, vol. 478, pp. 522–531, 2019, doi: 10.1016/j.apsusc.2019.02.004.

[48] H. D. Bui, H. R. Jappor, and N. N. Hieu, "Tunable optical and electronic properties of Janus monolayers Ga_2SSe, Ga_2STe, and Ga_2SeTe as promising candidates for ultraviolet photodetectors applications," Superlattices and Microstructures, vol. 125, pp. 1–7, 2019, doi: 10.1016/j.spmi.2018.10.020.

[49] A. Huang, W. Shi, and Z. Wang, "Optical properties and photocatalytic applications of two-dimensional Janus group-III monochalcogenides," The Journal of Physical Chemistry C, vol. 123, no. 18, pp. 11388–11396, 2019, doi: 10.1021/acs.jpcc.8b12450.

[50] H. R. Jappor, M. M. Obeid, T. V. Vu, D. M. Hoat, H. D. Bui, N. N. Hieu, and R. Khenata, "RETRACTED: engineering the optical and electronic properties of Janus monolayer Ga_2SSe by biaxial strain," Superlattices and Microstructures, vol. 125, p. 105031, 2019, doi: 10.1016/j.

spmi.2019.05.031.

[51] G. Guo, G. Zhang, H. Wu, Y. Zhang, and Z. Xie, "Insights on the optoelectronic properties in two-dimensional Janus lateral In_2SeTe/Ga_2STe heterostructure," Thin Solid Films, vol. 718, p. 138479, 2021, doi: 10.1016/j.tsf.2020.138479.

[52] P. Giannozzi, S. Baroni, N. Bonini, M. Calandra, R. Car, C. Cavazzoni, A. D. Corso, S. Giannozzi, M. de Gironcoli, F. (Giannozzi), A. Kokalj, and R. M. Wentzcovitch, "QUANTUM ESPRESSO: a modular and open-source software project for quantum simulations of materials," Journal of Physics: Condensed Matter, vol. 21, no. 39, p. 395502, 2009, doi: 10.1088/0953-8984/21/39/395502.

[53] P. E. Blöchl, "Projector augmented-wave method," Physical Review B, vol. 50, no. 24, p. 17953, 1994, doi: 10.1103/PhysRevB.50.17953.

[54] J. P. Perdew, K. Burke, and M. Ernzerhof, "Generalized gradient approximation made simple," Physical Review Letters, vol. 77, no. 18, p. 3865, 1996, doi: 10.1103/PhysRevLett.77.3865.

[55] J. Heyd, G. E. Scuseria, and M. Ernzerhof, "Hybrid functionals based on a screened Coulomb potential," The Journal of Chemical Physics, vol. 118, no. 18, pp. 8207–8215, 2003, doi: 10.1063/1.1564060.

[56] H. J. Monkhorst and J. D. Pack, "Special points for Brillouin-zone integrations," Physical Review B, vol. 13, no. 12, p. 5188, 1976, doi: 10.1103/PhysRevB.13.5188.

[57] A. Marini, C. Hogan, M. Grüning, and D. Varsano, "Yambo: an ab initio tool for excited state calculations," Computer Physics Communications, vol. 180, no. 8, pp. 1392–1403, 2009, doi: 10.1016/j.cpc.2009.02.003.

[58] M. Ait Tamerd, M. Zanouni, A. Nid-bahami, M. Diani, and A. Marjaoui, "Strain effects on the structural, electronic, optical and thermoelectric properties of Si_2SeS monolayer with puckered honeycomb structure: A first-principles study," International Journal of Quantum Chemistry, vol. 122, no. 13, p. e26906, 2022, doi: 10.1002/qua.26906.

[59] A. Kokalj, "XCrySDen—a new program for displaying crystalline structures and electron densities," Journal of Molecular Graphics and Modelling, vol. 17, no. 3-4, pp. 176–179, 1999, doi: 10.1016/S1093-3263(99)00028-5.

[60] Y. Guo, S. Zhou, Y. Bai, and J. Zhao, "Enhanced piezoelectric effect in Janus group-III chalcogenide monolayers," Applied Physics Letters, vol. 110, no. 16, 2017, doi: 10.1063/1.4981877.

[61] P. Hu, L. Wang, M. Yoon, J. Zhang, W. Feng, X. Wang, and K. Xiao, "Highly responsive ultrathin GaS nanosheet photodetectors on rigid and flexible substrates," Nano Letters, vol. 13, no. 4, pp. 1649–1654, 2013, doi: 10.1021/nl400107k.

[62] G. W. Mudd, S. A. Svatek, L. Hague, O. Makarovsky, Z. R. Kudrynskyi, C. J. Mellor, and A. Patanè, "High broad-band photoresponsivity of mechanically formed InSe–graphene van der Waals heterostructures," Advanced Materials (Deerfield Beach, Fla.), vol. 27, no. 25, p. 3760, 2015, doi: 10.1002/adma.201500889.

[63] Z. Hussein, A. Laref, H. R. Alqahtani, E. A. Alghamdi, M. E. A. Monir, N. A. Noor, and H. A. Yakout, "Optoelectronic properties of solar cell materials based on copper-zinc-tin-sulfide Cu2ZnSn(SxTe1-x)4 alloys for photovoltaic device applications," Solar Energy, vol. 225, pp. 851–862, 2021, doi: 10.1016/j.solener.2021.07.019.

[64] Z. Hui, X. Tang, R. Wei, L. Hu, J. Yang, H. Luo, X. Zhang, Y. Yang, and Y. Sun, "Facile chemical solution deposition of nanocrystalline CrN thin films with low magnetoresistance," RSC Advances, vol. 4, no. 24, pp. 12568–12571, 2014, doi: 10.1039/C4RA00263F.

[65] B. T. Beshir, K. O. Obodo, and G. A. Asres, "Janus transition metal dichalcogenides in

combination with MoS2 for high-efficiency photovoltaic applications: A DFT study," RSC Advances, vol. 12, no. 22, pp. 13749–13755, 2022, doi: 10.1039/D2RA00775D.

[66] B. J. Wang, X. H. Li, R. Zhao, X. L. Cai, W. Y. Yu, W. B. Li, and S. H. Ke, "Electronic structures and enhanced photocatalytic properties of blue phosphorene/BSe van der Waals heterostructures," Journal of Materials Chemistry A, vol. 6, no. 19, pp. 8923–8929, 2018.

[67] T. A. Alrebdi and B. Amin, "Van der Waals heterostructure of Janus transition metal dichalcogenides monolayers (WSSe-WX2 (X = S, Se))," Chemical Physics, vol. 549, p. 111252, 2021, doi: 10.1016/j.chemphys.2021.111252.

[68] R. González-Reyes, J. D. Correa, F. M. Nava-Maldonado, K. A. Rodríguez-Magdaleno, M. E. Mora-Ramos, and J. C. Martínez-Orozco, "Black Phosphorene/MoS2 van der Waals heterostructure: Electronic and optical properties," Physica B: Condensed Matter, vol. 673, p. 415489, 2024, doi: 10.1016/j.physb.2023.415489.

[69] Y. Zhao, Q. Tan, H. Li, Z. Li, Y. Wang, and L. Ma, "Tunable electronic and photoelectric properties of Janus group-III chalcogenide monolayers and based heterostructures," Scientific Reports, vol. 14, no. 1, p. 10698, 2024, doi: 10.1038/s41598-024-61373-z.

[70] S. V. Eremeev, M. Papagno, I. Grimaldi, O. De Luca, L. Ferrari, A. K. Kundu, G. Autès, L. Moreschini, A. Crepaldi, M. Battiato, O. V. Yazyev, F. Parmigiani, and D. Pacilè, "Insight into the electronic structure of semiconducting ε-GaSe and ε-InSe," Physical Review Materials, vol. 4, no. 8, p. 084603, Aug. 2020, doi: 10.1103/PhysRevMaterials.4.084603.

[71] J. Zhou, J. Shi, Q. Zeng, Y. Chen, L. Niu, F. Liu, Y. Wang, D. Huang, Y. Cai, H. Lin, S. T. Pantelides, and Z. Liu, "InSe monolayer: synthesis, structure and ultra-high second-harmonic generation," 2D Materials, vol. 5, no. 2, p. 025019, Mar. 2018, doi: 10.1088/2053-1583/aab390.

[72] H. R. Jappor and M. A. Habeeb, "Tunable electronic and optical properties of GaS/GaSe van der Waals heterostructure," Current Applied Physics, vol. 18, no. 6, pp. 673–680, June 2018, doi: 10.1016/j.cap.2018.03.019.

[73] F. Opoku, A. Aniagyei, O. Akoto, E. E. Kwaansa-Ansah, N. K. Asare-Donkor, and A. A. Adimado, "Investigation of 2D Janus Al_2OS/Ga_2SSe van der Waals heterojunction as next-generation thermoelectric and photocatalytic devices," Next Materials, vol. 1, no. 4, p. 100042, Dec. 2023, doi: 10.1016/j.nxmate.2023.100042.

[74] S. S. Ullah, M. Farooq, H. U. Din, Q. Alam, M. Idrees, M. Bilal, and B. Amin, "First principles study of electronic and optical properties and photocatalytic performance of GaN–SiS van der Waals heterostructure," RSC Advances, vol. 11, no. 52, pp. 32996–33003, Sept. 2021, doi: 10.1039/D1RA06011B.

[75] H. T. Do, T. V. Vu, A. A. Lavrentyev, N. Q. Cuong, P. V. Cuong, and H. D. Tong, "Electronic structure and interface contact of two-dimensional van der Waals boron phosphide/Ga_2SSe heterostructures," RSC Advances, vol. 12, no. 30, pp. 19115–19121, Aug. 2022, doi: 10.1039/D2RA02748H.

[76] C. He, F. S. Han, J. H. Zhang, and W. X. Zhang, "The In_2SeS/gC_3N_4 heterostructure: A new two-dimensional material for photocatalytic water splitting," Journal of Materials Chemistry C, vol. 8, no. 20, pp. 6923–6930, May 2020, doi: 10.1039/D0TC00852D.

[77] S. Rühle, "Tabulated values of the Shockley–Queisser limit for single-junction solar cells," Solar Energy, vol. 130, pp. 139–147, 2016, doi: 10.1016/j.solener.2016.02.015.

[78] M. H. Dalsaniya, T. K. Gajaria, N. N. Som, P. K. Jha, P. Śpiewak, and K. J. Kurzydłowski, "Type-II GeAs/GaSe heterostructure as suitable candidate for solar power conversion efficiency," Solar Energy, vol. 223, pp. 87–99, May 2021, doi: 10.1016/j.solener.2021.05.034.

[79] X. H. Li, B. J. Wang, H. Li, X. F. Yang, R. Q. Zhao, X. T. Jia, and S. H. Ke, "Two-dimensional layered Janus-In_2SeTe/C_2N van der Waals heterostructures for photocatalysis and photovoltaics: first-principles calculations," New Journal of Chemistry, vol. 44, no. 37, pp. 16092–16100, Oct. 2020, doi: 10.1039/D0NJ03296D.

[80] T. Z. Wen, Y. H. Yang, and J. L. Li, "A novel Black-P/Blue-P heterostructure for the photovoltaic applications," Chemical Physics Letters, vol. 812, p. 140242, Jan. 2023, doi: 10.1016/j.cplett.2022.140242.

[81] Y. Ding, S. Fang, H. Zhou, J. Qi, J. Fan, R. Zhang, Y. Wang, J. Liu, X. Chen, L. Sun, and H. Tang, "High-performance type II WSOx/WS_2-based heterojunction photodetectors," Applied Surface Science, vol. 683, p. 161848, 2025, doi: 10.1016/j.apsusc.2024.161848.

[82] Z. Guan, C. S. Lian, S. Hu, S. Ni, J. Li, and W. Duan, "Tunable structural, electronic, and optical properties of layered two-dimensional C_2N and MoS_2 van der Waals heterostructure as photovoltaic material," The Journal of Physical Chemistry C, vol. 121, no. 6, pp. 3654–3660, 2017, doi: 10.1021/acs.jpcc.6b12681.

[83] Y. Xu, D. Li, Q. Zeng, H. Sun, and P. Li, "Type-II 2D AgBr/SiH van der Waals heterostructures with tunable band edge positions and enhanced optical absorption coefficients for photocatalytic water splitting," RSC Advances, vol. 13, no. 40, pp. 27676–27685, 2023, doi: 10.1039/D3RA05079C.